Theory of Multiphonon Absorption in Insulating Crystals*

M. Sparks
Xonics, Incorporated, Van Nuys, California 91406

L. J. Sham
University of California, San Diego, La Jolla, California 92037
Xonics, Incorporated, Van Nuys, California 91406

(Received 16 March 1973)

The nearly exponential frequency dependence of the infrared-absorption coefficient β recently observed in 15 crystals up to several times the reststrahl frequency is explained in terms of multiphonon-absorption processes. The central-limit theorem is used to reduce the multiphonon contribution to a simple closed form. The theoretical estimates for the magnitude of the absorption coefficient, with no adjustable parameters, are also in good agreement with experiment. The temperature dependence of β at a fixed frequency is shown to be considerably weaker than $\beta \sim T^{n-1}$, where n is the number of created phonons. Higher-order processes in the perturbation expansion are shown to be negligible for small n, to be comparable to that of the lowest-order, single-vertex terms for $n \cong 5$, and to dominate for large n in a typical case. Difference processes, in which some thermally excited phonons are annihilated, are shown to be negligible with respect to the summation processes in the nearly exponential region. An explanation involving finite phonon lifetimes is proposed to explain the fact that the alkali halides show less structure in the β-ω curves than do the semiconductor crystals.

I. INTRODUCTION

The intensity I of infrared radiation propagating through a solid typically decays according to Beer's law, $I = I_0 e^{-\beta x}$, where β is defined as the optical-absorption coefficient. Extensive experimental and theoretical studies have been conducted on the absorption due to phonons in insulating or semiconducting crystals. References 1–4 represent some recent reviews on this topic. The main interest has been focused on the two-phonon region where $\beta \gg 1$ cm^{-1}, and particularly on the structure of the frequency dependence that determines the critical points of the phonon spectra.[5] The availability of high-power infrared lasers has shifted attention to higher-order phonon processes, where $\beta \ll 1$ cm^{-1}. Not only the positions of the multiphonon peaks are of interest, but also the magnitude of β is of great importance now that high intensities are available.

It has been observed[6,7(a),7(b)] that for frequencies ω greater than several times the reststrahl frequency ω_f, the optical-absorption coefficient varies nearly exponentially with frequency,

$$\beta \sim e^{-A\omega} , \tag{1.1}$$

for a number of crystals including LiF, NaF, NaCl, KCl, KBr, MgF_2, CaF_2, BaF_2, SrF_2, MgO, Al_2O_3, SiO_2, TiO_2, $BaTiO_3$, and $SrTiO_3$. This is true for $\beta \lesssim 10$ cm^{-1} and $\omega \gtrsim 2\omega_f$, roughly. In NaCl at room temperature, for instance, β decreases nearly exponentially for over four orders of magnitude as the frequency increases from $2.2\omega_f$ to $5.8\omega_f$, as shown in Fig. 1.

At first sight, the nearly exponential behavior might suggest the form $\beta \sim e^{-\hbar\omega/k_B T}$. However, the room-temperature values of the coefficient A in (1.1) differ by factors of 2–4 from the value of $\hbar/k_B T$. Furthermore, the temperature dependence[8] of β, though not extensively studied to date, appears to be less strong than $e^{-\hbar\omega/k_B T}$.

In this paper, an investigation of the optical absorption by multiphonon processes is presented. It is shown that the sum of n-phonon summation processes is approximately exponentially decreasing with increasing frequency over the frequency range of interest, i.e. about $2\omega_f$ to $7\omega_f$, typically. As illustrated in Fig. 2(a), we consider the n-phonon summation process in which the photon is absorbed by the crystal through the virtual excitation of the fundamental reststrahlen mode which finally emits n phonons. In other words, the electromagnetic field drives the fundamental mode (off resonance since $\omega > \omega_f$), whose relaxation time is determined by the sum of all possible processes of splitting into n normal modes of lattice vibrations. The Lax-Burstein-Born higher-order dipole-moment mechanism[9] is not considered explicitly, although most of the analysis still applies to that case.

By energy conservation, the energy $\hbar\omega$ of the photon absorbed is equal to the sum of the energies of the n final-state phonons. It follows that the n-phonon summation process cannot contribute to β when $\omega > n\omega_{gr}$, where ω_{gr} is the greatest frequency of the phonon spectrum. For $\omega \ll n\omega_{gr}$, the contribution β_n of the n-phonon summation process to β is small because the low frequencies of the

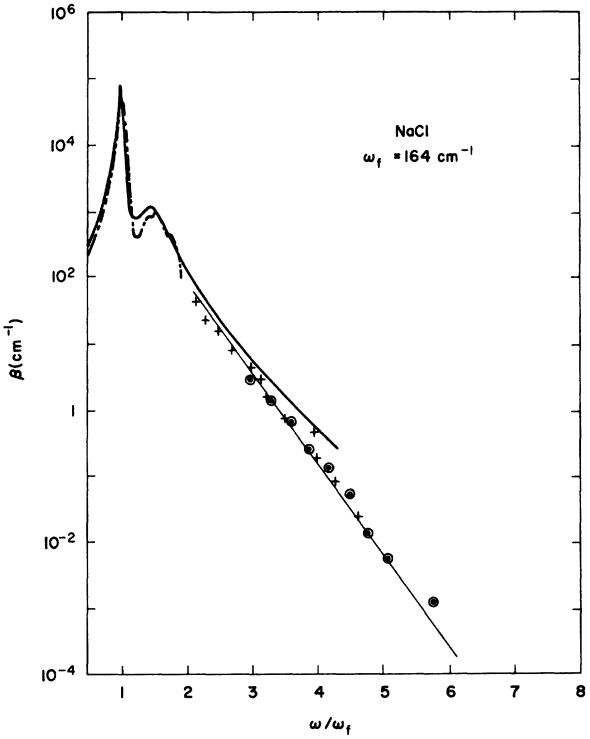

FIG. 1. Experimental frequency dependence of the infrared absorption coefficient β for NaCl after Horrigan and Deutsch (+, ⊙) Ref. 7(a), Smart *et al.* (– · –) Ref. 7(c) and Genzel (–) Ref. 7(d).

final-state phonons greatly restrict the amount of phase space available. Thus, β_n must peak at a frequency not far below $n\omega_{gr}$. As n increases, the peak shifts to higher frequencies and decreases in height since higher-order phonon processes involve weaker coupling coefficients. The sum of the β_n then has a frequency dependence nearly exponential in the experimental frequency range. This behavior of the β_n and the sum of the β_n is demonstrated explicitly in Sec. VI.

A preliminary account of these results has been published.[10] Subsequent investigations are discussed in Sec. II. The exponential frequency dependence of the absorption was first suggested by Rupprecht[6] to be due to n-phonon processes, although he did not investigate the theory in detail.

In Sec. II, formal expressions for the contribution to β due to multiphonon processes are given. A practical approximation for the anharmonic coefficient is chosen. In Sec. III, an asymptotic approximation for evaluation of the n-phonon contribution is developed. In Sec. IV, confluence phonon processes are shown to be unimportant in the nearly exponential region. In Sec. V, all possible processes that convert the fundamental phonon to n phonons are examined, and the contributions of vertex corrections are estimated. In Sec. VI, the explicit evaluation of β_n is described, and comparison of theory with experiment is made. In Sec. VII, a summary of all the assumptions and approximations that have gone into the theory is given, and the relation of a computer-calculation program to the present results is discussed.

II. ANHARMONIC CONTRIBUTION TO ABSORPTION COEFFICIENT

The infrared radiation perturbs the insulating crystal by excitation of the dipole moment of the crystal by the oscillating electric field. The absorption coefficient is simply related to the imaginary part of the electric susceptibility by

$$\beta(\omega) = 4\pi\chi_I(\omega)\omega/n_r c \ , \qquad (2.1)$$

where c is the speed of light and n_r is the refractive index at frequency ω. The susceptibility, in turn, is just the linear response of the dipole moment.[3,11] In an anharmonic crystal, the dipole moment can be expanded in powers of the ionic displacements.[12] For infrared-active crystals, the leading nonzero term is linear in the ionic displacements. The nonlinear terms (the dominant mechanism for infrared absorption in such non-infrared-active crystals as diamond[9]) are probably small in polar crystals, especially in alkali halides,[13,14] and shall be neglected in this work. However, there are contrary conclusions.[15]

Then, the absorption coefficient is given by the

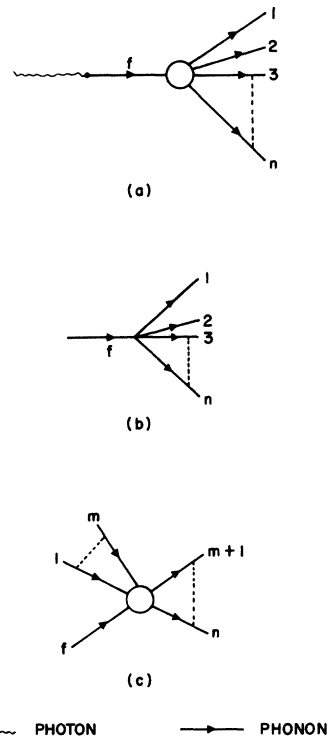

FIG. 2. n-phonon summation and confluence processes.

imaginary part of the Green's function of the fundamental mode,[3,13]

$$\beta=\frac{4\pi Ne^{*2}}{cm_r n_r \Omega}\frac{\omega\omega_f\Gamma(\omega)}{(\omega^2-\omega_f^2)^2+[\omega_f\Gamma(\omega)]^2}\ , \tag{2.2}$$

where N is the number of unit cells, Ω is the volume of the crystal, e^* is the Born effective charge, m_r is the reduced mass of the two ions in the unit cell, and Γ is the energy relaxation frequency of the fundamental mode (equal to twice the Γ in R. A. Cowley's notation[13]). The real part of the phonon self-energy is understood to have been included in producing the renormalized reststrahl frequency ω_f, and its frequency dependence is neglected in Eq. (2.2). A simple classical model of a harmonic oscillator (the fundamental lattice mode) driven by the applied electric field gives (2.2), but with $\omega_f\Gamma$ replaced by $\omega\Gamma$ in the numerator and denominator.[12]

The contribution Γ_n from the n-phonon summation processes to Γ can be calculated by applying[16] the standard perturbation-theory result that the probability per unit time of a transition between two states is $2\pi/\hbar$ times the product of the square of the matrix element and the energy-conserving δ function, giving

$$\Gamma_n(\omega)=\frac{2\pi}{\hbar^2}(n+1)^2 n!\sum_{Q_1\cdots Q_n}|\Lambda(fQ_1\cdots Q_n)|^2 \times\Delta\left(\sum_{j=1}^{n}\vec{q}_j\right)\delta\left(\omega-\sum_{j=1}^{n}\omega_{Q_j}\right)\tilde{n}_n\ , \tag{2.3}$$

where Q_j is the phonon mode with wave vector $\vec{q}_j$ and branch b_j, Δ is the modified Kronecker δ which is unity when the argument is zero or a reciprocal-lattice vector and zero otherwise, and

$$\tilde{n}_n=\prod_{j=1}^{n}\frac{n_j+1}{n_\omega+1}\ , \tag{2.4}$$

with

$$n_j=n(Q_j)=1/(e^{\omega_{Q_j}/\omega_T}-1)\ , \tag{2.5}$$

$$n_\omega=1/(e^{\omega/\omega_T}-1)\ , \tag{2.6}$$

and

$$\omega_T=k_B T/\hbar\ . \tag{2.7}$$

Furthermore, $\Lambda(fQ_1\cdots Q_n)$ denotes the renormalized $(n+1)$-phonon vertex, represented by the circle in Fig. 2(a), and is the sum of all possible $(n+1)$-phonon vertices. The simplest one is the unrenormalized vertex $V(fQ_1\cdots Q_n)$ from the anharmonic Hamiltonian given by[12,13]

$$\mathcal{H}_{n+1}=\sum_{Q_1}\cdots\sum_{Q_{n+1}}V(Q_1\cdots Q_{n+1})\Delta\left(\sum_{j=1}^{n+1}\vec{q}_j\right)A_{Q_1}\cdots A_{Q_{n+1}}\ , \tag{2.8}$$

where

$$A_Q\equiv A_{\vec{q}b}=a_{\vec{q}b}+a^\dagger_{-\vec{q}b}\ , \tag{2.9}$$

with $a^\dagger$ and a being the phonon creation and annihilation operators normalized to unit commutators, as usual. This simple vertex is represented diagrammatically in Fig. 2(b). Other more complicated processes are examined in Sec. V, where we derive an approximate form for the total vertex

$$\Lambda(fQ_1\cdots Q_n)=\Lambda_n V(fQ_1\cdots Q_n)\ . \tag{2.10}$$

To obtain a reasonable approximation for the anharmonic coefficients, let us confine our attention to diatomic polar crystals with cubic symmetry, especially NaCl-structure crystals. The model interaction potential[12,17] between ions is composed of a Coulomb potential and a nearest-neighbor overlap exchange repulsion of the form

$$\phi(r)=Ce^{-r/\rho a}\ , \tag{2.11}$$

where a is the equilibrium nearest-neighbor distance. The Coulomb interaction is used only in determining the constants C and ρ in Eq. (2.11) from the equilibrium condition and the value of the bulk modulus, B, yielding[12,17]

$$C=3a^3Be^{1/\rho}\rho^2/(1-2\rho)\ . \tag{2.12}$$

In the anharmonic coefficients, only the derivatives of the repulsive potential (2.11) are retained. Since ρ is of the order of 0.1 for NaCl, the derivatives of the Coulomb potential are smaller than the corresponding ones of the repulsive potential for orders up to at least $n\cong 10$. Had we used an inverse power law for the repulsive potential, this would be true to any order. This model, including the neglect of the Coulomb potential in the anharmonic terms, has been used previously[13] with much success.

The anharmonic coefficients can be obtained in a straightforward calculation from this nearest-neighbor exchange repulsion potential.[12] The mth-order coefficient $V(Q_1\cdots Q_m)$ involves derivatives of $\phi(r)$ up to order m. From the exponential form (2.11), it is clear that

$$|a\phi^{(m)}(a)/\phi^{(m-1)}(a)|\sim 10\ . \tag{2.13}$$

Thus, it is a good approximation to retain only the highest-order derivative. Using these results and assuming central forces yield

$$V(Q_1\cdots Q_m)=\frac{N}{m!}\phi^{(m)}(a)\sum_{\gamma=1}^{6}\prod_{j=1}^{m}U_\gamma(Q_j)\left(\frac{\hbar}{2Nm_<\omega_{Q_j}}\right)^{1/2}, \tag{2.14}$$

where

$$U_\gamma(Q_j)=\hat{x}_\gamma\cdot[\vec{w}_{<Q_j}-(m_</m_>)^{1/2}\vec{w}_{>Q_j}e^{i\vec{q}\cdot\vec{x}_\gamma}]\ , \tag{2.15}$$

and $m_<$ and $m_>$ denote the smaller and larger ionic masses, respectively. The positions of nearest neighbors measured from the lighter ion are $\vec{x}_\gamma$, and $\hat{x}_\gamma$ is the unit vector in the same direction. The polarization vector $\vec{w}_{<Q}$ is defined in terms of

the ionic displacement $\vec{u}_{l\tau}$ from the equilibrium position $\vec{x}_{l\tau}$ by the relation[12,18]

$$\vec{u}_{l\tau}=\sum_{Q}(\hbar/2Nm_\tau\omega_Q)^{1/2}e^{i\vec{q}\cdot\vec{x}_{l\tau}}A_Q\vec{w}_{\tau Q}\ , \qquad (2.16)$$

with τ denoting the ion type. For the fundamental mode,

$$U_\gamma(f)=\hat{x}_\gamma\cdot\hat{w}_f(m_</m_\tau)^{1/2}\ , \qquad (2.17)$$

with $m_\tau=(m_<^{-1}+m_>^{-1})^{-1}$. From Eq. (2.11), we obtain the mth derivative

$$\phi^{(m)}(a)=\frac{3Ba^3\rho^2}{(1-2\rho)(-\rho a)^m}\ . \qquad (2.18)$$

Substituting the approximate expression (2.14) for the anharmonic coefficient into Eq. (2.3) for Γ_n, we obtain, by using Eq. (2.2), the contribution of the n-phonon summation process to the optical absorption in the form

$$\beta_n=(\tfrac{1}{2}\pi)^{1/2}K\omega_{mx}^5D_\rho(1-e^{-\omega/\omega_T})(\omega^4n!)^{-1}\times(\omega_{mx}D_e)^n\Lambda_n^2\Sigma_n\ . \qquad (2.19)$$

We have used the approximation for high frequency ($\omega^2\gg\omega_f^2+\Gamma^2$) and introduced the following groups of constants:

$$K=\frac{B^2e^{*2}a\omega_f}{\hbar cm_\tau^2n_\tau\omega_{mx}^5}\ ,$$
$$D_\rho=(2\pi)^{-1/2}[6\pi\rho/(1-2\rho)]^2\ , \qquad (2.20)$$
$$D_e=\hbar/2\rho^2a^2m_<\omega_{mx}\ .$$

The frequency ω_{mx}, introduced for later use, cancels out in Eq. (2.19).

The factor Σ_n contains the dynamical information of the n-phonon absorption and is given by

$$\Sigma_n=\sum_{\gamma=1}^{6}\sum_{\gamma'=1}^{6}(\hat{x}_\gamma\cdot\hat{w}_f)(\hat{x}_{\gamma'}\cdot\hat{w}_f)N^{-n}\times\sum_{Q_1\cdots Q_n}N\Delta\left(\sum_{j=1}^{n}q_j\right)\delta\left(\omega-\sum_{j=1}^{n}\omega_{Q_j}\right)\times\prod_{j=1}^{n}U_\gamma(Q_j)U_{\gamma'}^*(Q_j)\frac{n(\omega_{Q_j})+1}{\omega_{Q_j}}\ . \qquad (2.21)$$

For crystals of NaCl structure, symmetry[19(a)] ensures that Σ_n and, therefore, β_n are independent of the direction of $\hat{w}_f$. Let us choose $\hat{w}_f$ to be along the positive x axis. Then, Eq. (2.21) becomes

$$\Sigma_n=2\Sigma_{n+}+2(-1)^{n+1}\Sigma_{n-}\ , \qquad (2.22)$$

where

$$\Sigma_{n\pm}=N^{-n}\sum_{Q1\cdots Q_n}N\Delta\left(\sum_{j=1}^{n}\vec{q}_j\right)\delta\left(\omega-\sum_{j=1}^{n}\omega_{Q_j}\right)\times\prod_{j=1}^{n}W_\pm(Q_j)\frac{n_{Q_j}+1}{\omega_{Q_j}} \qquad (2.23)$$

and, with Re and Im denoting real and imaginary parts, respectively,

$$W_\pm(Q)=[\mathrm{Re}\,U_x(Q)]^2\pm[\mathrm{Im}\,U_x(Q)]^2\ . \qquad (2.24)$$

In passing, note that the evaluation of the sums in (2.23) is trivial if the density of states $g(\omega)$ is approximated by the Einstein model

$$g(\omega)=\delta(\omega-\omega_E)$$

and the angle dependence of $W_\pm(Q)$ is neglected: $W_\pm(Q)=W_\pm$. It will be shown later that $W_+^n\gg W_-^n$. Then (2.23) and (2.19) give directly

$$\beta=\sum_{n=1}^{\infty}\frac{E\Lambda_n^2}{n^4n!}(1-e^{-n\omega_E/\omega_T})\left(\frac{6\omega_{mx}D_eW_+[n(\omega_E)+1]}{\omega_E}\right)^n\times\delta(\omega-n\omega_E)\ , \qquad (2.25)$$

where $E\equiv(2\pi)^{1/2}K\omega_{mx}D_\rho$. According to (2.25), the spectrum is approximated by a series of δ functions, which is, of course, not realistic. Even though such a model is not of significant practical value, it does crudely approximate some of the features of the more realistic model discussed below. For example, plotting the coefficients of the δ functions in (2.25), or formally replacing the δ functions by line-shape functions of finite width, gives a nearly exponential decrease with increasing frequency. In Ref. 19(b), the result (2.25) was rederived using the simpler model of a one-dimensional lattice with the Einstein approximation and a simpler interaction potential that neglects the angle dependence [our factor $W_\pm(Q)$] from the outset, and an independent-molecule model was considered. Use of this simpler interaction potential gives unreasonably large values of Λ_n^2, which causes noticeable deviation from an exponential frequency dependence.[19(b)]

Mills and Maradudin[19(c)] independently used a single-frequency anharmonic-molecule-type lattice to study various types of interaction potentials, effects of impurities, and high-temperature effects. Bendow, Ying, and Yukon[19(d)] have used a different mathematical method that starts with partially summed terms. The method is potentially powerful, but to date they have recovered only our terms without the vertex correction. Since the validity of the perturbation expansion is justified by showing that all diagrams not included in the result are negligible, it is expected that new methods of calculation should give equivalent results. For example, the factor $e^{-\gamma T}$ resulting from vertices with phonon loops[19(d)] [A_QA_QS, $A_QA_{Q'}A_{Q'}S$, etc., where S is the simple vertex and the A_Q are defined in (2.9)] is well approximated by 1 since the phonon-loop terms are negligible with respect to simple vertices (see Sec. V).

III. ASYMPTOTIC APPROXIMATION FOR ABSORPTION BY LARGE NUMBER OF PHONONS

Equation (2.19) gives the contribution to the absorption coefficient by the n-phonon summation process. It contains the factor Σ_n given by Eqs. (2.22)–(2.24) which involves n-fold Brillouin-zone sums. Although these are not beyond the means of modern computing capabilities for n in the experimental range of 2–8, we are still interested in analytical approximations that will give us general properties of β which appear to be shared by a rather large number of crystals. The method of evaluation used in this section is correct in the large-n limit.

For $n \gtrsim 2$ we can neglect the quasi-momentum-conservation restriction in the sums given by Eq. (2.23). We shall justify this later in this section. First note that if the angle dependence of $W_\pm(Q_j)$ is neglected, the summand in (2.23) is a function of phonon frequencies ω_{Q_j} only. Then, replacing the sums over Q_j by integrals over $d\omega_{Q_j} g(\omega_{Q_j})$, where $g(\omega_{Q_j})$ is the phonon density of states, reduces (2.23) to the form

$$\Sigma_{n\pm} = \int d\omega_{Q_1} f(\omega_{Q_1}) \cdots \int d\omega_{Q_n} f(\omega_{Q_n}) \delta\left(\omega - \sum_{j=1}^{n} \omega_{Q_j}\right) ,$$

to which the central-limit theorem applies directly. Here $f(\omega_{Q_j}) = 6N^{-1} W_\pm(Q_j)(n_{Q_j}+1) g(\omega_{Q_j})/\omega_{Q_j}$, where the normalization constant $6N^{-1}$ arises since g is normalized to unity.

Equation (2.23) can be cast into this central-limit-theorem form without neglecting the angle dependence of $W_\pm(Q_j)$ as follows: We introduce two functions which are kindred to the phonon propagators

$$\sigma_\pm(\zeta) = (\omega_{mx}/N\alpha_{0\pm}) \sum_Q W_\pm(Q)[(n_Q+1)/\omega_Q]\delta(\zeta - \omega_Q) , \tag{3.1}$$

where

$$\alpha_{0\pm} = \omega_{mx} N^{-1} \sum_Q W_\pm(Q)(n_Q+1)/\omega_Q \tag{3.2}$$

are constants for normalizing the integrals of $\sigma_\pm(\zeta)$ over ζ to unity.

The n-fold sums in Eq. (2.23) can be written as n-dimensional integrals,

$$\Sigma_{n\pm} = \left(\frac{\alpha_{0\pm}}{\omega_{mx}}\right)^n \int_{-\infty}^{\infty} d\zeta_1 \sigma_\pm(\zeta_1) \cdots \times \int_{-\infty}^{\infty} d\zeta_n \sigma_\pm(\zeta_n) \delta\left(\omega - \sum_{j=1}^{n} \zeta_j\right) . \tag{3.3}$$

These convolution integrals are well known in statistics. For $n \to \infty$, the integral tends to a Gaussian (the central-limit theorem),

$$\Sigma_{n\pm} = \left(\frac{\alpha_{0\pm}^n}{(2\pi n)^{1/2} \alpha_{2\pm} \omega_{mx}^{n+1}}\right) \exp\left(\frac{-(\omega - n\alpha_{1\pm}\omega_{mx})^2}{2n\alpha_{2\pm}^2 \omega_{mx}^2}\right), \tag{3.4}$$

where $\alpha_{0\pm}$ are defined in Eq. (3.2), and

$$\alpha_{1\pm} = \omega_{mx}^{-1} \int_{-\infty}^{\infty} d\zeta \, \sigma_\pm(\zeta)\zeta , \tag{3.5}$$

$$(\alpha_{2\pm}\omega_{mx})^2 = \int_{-\infty}^{\infty} d\zeta \, \sigma_\pm(\zeta)\zeta^2 - (\alpha_{1\pm}\omega_{mx})^2 . \tag{3.6}$$

For small n, it is possible to improve Eq. (3.4) with an asymptotic series.[20] A particular series in terms of Hermite polynomials has been used by Sjolander[21] to evaluate the multiphonon background in neutron scatterings in a harmonic crystal.

It is obvious from Eq. (2.24) that α_{0-}, as defined by Eq. (3.2), is less than α_{0+}. The estimates discussed in Sec. IV show that α_{0-} is about one-third to one-half of α_{0+}, at most. Since $\Sigma_{0\pm} \sim (\alpha_{0\pm})^n$ according to (3.4), Σ_{n-} becomes negligible compared with Σ_{n+} for large n. Therefore, from Eqs. (2.19), (2.22), and (3.4), the absorption coefficient has the explicit form

$$\beta_n = \frac{D_\rho K}{\alpha_{2+}(n_\omega+1)} \left(\frac{\omega_{mx}}{\omega}\right)^4 \frac{1}{n^{1/2} n!} (\alpha_{0+} D_e)^n \Lambda_n^2 \times \exp\left(\frac{-(\omega - n\alpha_{1+}\omega_{mx})^2}{2n(\alpha_{2+}\omega_{mx})^2}\right) . \tag{3.7}$$

By virtue of the central-limit theorem, the multiple sum over $Q_1, \cdots, Q_n$ has been reduced to sums over a single phonon coordinate Q_1, as given by Eqs. (3.2), (3.5), and (3.6).

The neglect of momentum conservation appears to be physically reasonable since, for larger and larger n, the restriction on phase space becomes less and less important. However, if we wish not to neglect the momentum conservation in Eq. (2.2), we can extend the foregoing procedure by treating the summations over $\vec{q}_j$ in the same manner as the integrals over ζ_j. Thus, we introduce the functions $\sigma_+(\vec{q}, \zeta)$ similar to Eq. (3.1), except omitting the sum over $\vec{q}$. Equation (3.3) becomes not only multiple integrals over ζ_j, but also over $\vec{q}_j$ with four δ functions, one for the frequency and three for the wave vectors. The convolution integral is evaluated in the same way by means of the central-limit theorem. The integrals over $\vec{q}_j$ contribute a factor which is a lattice sum of Gaussians of the form $e^{-n\alpha x_j^2}$ and is, therefore, approximately unity for large n. We arrive at the same answer as Eq. (3.4), thereby justifying the neglect of momentum conservation.

IV. CONFLUENCE PROCESSES

In the preceding calculation of the multiphonon absorption of light, only a particular type of phonon processes, called the n-phonon summation processes and illustrated in Fig. 2(a), was considered. We have neglected the confluence processes, illustrated in Fig. 2(c). Instead of creating n phonons after the annihilation of the fundamental

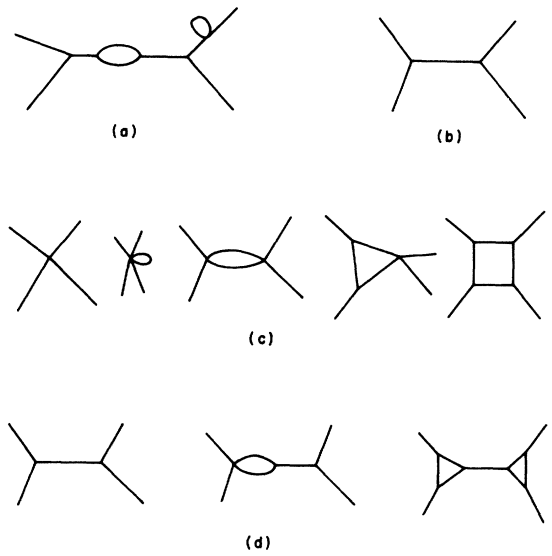

FIG. 3. Various kinds of vertices.

phonon, m phonons are absorbed, and $n-m$ phonons are created.

A confluence process involving n phonons (some of which are created and some annihilated) is governed by the same vertex as the n-phonon summation process. The contribution to the absorption coefficient of all confluence processes and the summation process is easily obtained by replacing $\delta(\zeta-\omega_Q)$ by $\delta(\zeta-\omega_Q)-\delta(\zeta+\omega_Q)$ and $n(-\omega_Q)$ by $-[n(\omega_Q)+1]$ in (3.1). The cross-product terms in (3.3) containing m factors of $-\delta(\zeta+\omega_Q)$ and $n-m$ factors of $\delta(\zeta-\omega_Q)$ correspond to the confluence process with m thermally excited phonons absorbed, as shown in Fig. 2(c). Applying the central-limit theorem to this term yields a Gaussian peaked at $(n-m)\alpha_{1+}\omega_{mx}-m\beta_{1+}\omega_{mx}$ instead of $n\alpha_{1+}\omega_{mx}$, where β_{1+} is defined by Eq. (3.5) with the new $\sigma_+(\zeta)$. This contribution will be masked by the summation process of $n-2m$ phonons which peaks at about the same frequency but has greater strength, being an anharmonic process of lower order.

V. VERTEX CORRECTIONS

Now we consider all possible processes that contribute to the $(n+1)$th-order vertex $\Lambda(fQ_1\cdots Q_n)$ and estimate the vertex correction factor Λ_n, defined by Eq. (2.10). Standard perturbation theory can be applied in a straightforward way to all the higher-order terms. For example, for $n=3$, the diagram in Fig. 4(b) below has one intermediate state. The contribution from this diagram is easily calculated, but it must be remembered that this diagram represents four diagrams when the arrow is added to the intermediate-state phonon. (There are two time orderings of the two vertices, and the arrow can go in either direction, corresponding to $aa^\dagger$ and $a^\dagger a$, in each time ordering.) This procedure has been carried out for a number of low-order diagrams,[10] and the results agree with those presented below.

Since the number of diagrams increases rapidly as n increases, this method becomes tedious and time consuming when applied to larger values of n. The following method is more convenient. First, all the self-energy corrections, such as those illustrated in Fig. 3(a), are taken to be accounted for by using the measured phonon frequencies, i.e., they are included in the corresponding "skeleton" diagram [Fig. 3(b)]. The lifetime of the intermediate- and final-state phonons is taken to be infinite.

There are two types of vertices: (i) the irreducible ones that cannot be rent asunder by cutting a single phonon line, such as those in Fig. 3(c), and (ii) the reducible ones that can be separated by cutting a single line, such as those in Fig. 3(d).

In the sum of all irreducible vertices of the same number of external phonon lines, the simple vertex dominates. We follow Van Hove[22] in ordering the anharmonic terms in the Hamiltonian, $V(Q_1\cdots Q_n)$, with ϵ^{n-2}, where ϵ is the small parameter given by the ratio of the root-mean-square displacement of the ions to the nearest-neighbor distance. The value of ϵ is less than 0.05 in alkali halides. A complex irreducible vertex must be of higher order in ϵ than the simple vertex with the same number of external lines, since cutting a phonon line will produce one vertex with a larger number of external lines. For example, the simple vertex in Fig. 3(c) is $O(\epsilon^2)$, but all the other irreducible vertices in Fig. 3(c) are $O(\epsilon^4)$.

On the other hand, a reducible vertex composed of simple irreducible vertices is of the same order in ϵ as the simple vertex with the same number of external lines. For example, the first diagram in Fig. 3(d) is $O(\epsilon^2)$. A reducible vertex that contains one or more complex irreducible vertices is again negligible. Therefore, for the total vertex contribution, we need only sum the simple vertex and the reducible vertices which are composed of simple vertices only.

To illustrate the procedure of obtaining the vertex renormalization to the n-phonon summation process, the simplest nontrivial vertex correction, namely, Λ_3, is first calculated. The two vertex terms that contribute to the three-phonon absorption are given in Figs. 4(a) and 4(b). The ratio of the latter to the simple vertex is

$$\frac{(3!)^2}{2!}\sum_{Q_4} V(fQ_3Q_4)D(Q_4,\zeta_4)V(Q_4Q_1Q_2)\Big/\frac{4!}{3!}V(fQ_1Q_2Q_3). \tag{5.1}$$

The two factors of 3! represent the number of ways[13,23] the phonon states are attached to the limbs of each vertex in Fig. 4(b). The divisor 2!

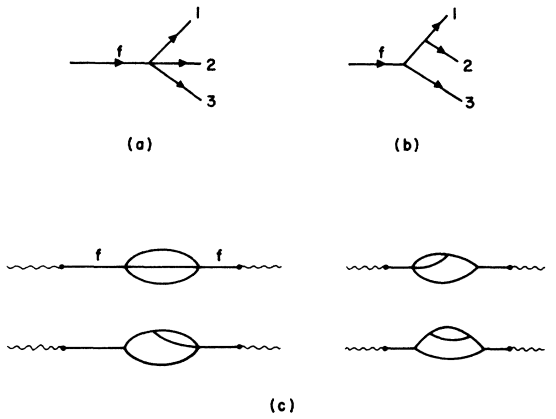

FIG. 4. Three-phonon summation processes.

represents the fact that interchanging the labels on phonon lines 1 and 2 again produces the same term. The factor 4! is the number of ways the four-phonon vertex in Fig. 4(a) can be labeled, and the divisor 3! is the overcounting factor generated by rearranging the labels among lines 1, 2, and 3 in Fig. 4(a). The factor $D(Q_4, \zeta_4)$ represents the Green's function for the intermediate phonon line[13,23] in Fig. 4(b).

By using the form (2.14) for the anharmonic coefficient and keeping only one term in the sum over nearest neighbors for both the numerator and the denominator of the ratio (5.1), we obtain the ratio

$$\frac{3!}{2!}\phi_{\backslash}^{(2)}\sum_{b_4}\frac{\hbar}{2m_{<}\omega_{Q_4}}\left|U_x(Q_4)\right|^2 D(Q_4,\zeta_4) \quad . \tag{5.2}$$

The factorial that represents the number of ways the states in each vertex are labeled cancels neatly the factorial in the anharmonic coefficient (2.14), leaving the counting factor in front of (5.2). This factor is just the ratio of the number of ways of rearranging the labels of the equivalent outgoing phonon lines of Fig. 4(a) to the corresponding number for Fig. 4(b).

The factor $\phi_{\backslash}^{(2)}$ comes from the fact that

$$(\phi_{\backslash}^{(3)})^2/\phi_{\backslash}^{(4)} = \phi_{\backslash}^{(2)} \tag{5.3}$$

by virtue of Eq. (2.18). The momentum and frequency of the intermediate-phonon Green's function are given by

$$\vec{q}_4 = \vec{q}_1 + \vec{q}_2 \tag{5.4}$$

and

$$\zeta_4 = \omega_f - \omega_3 = \omega_1 + \omega_2 \simeq 2\omega_{mx} \tag{5.5}$$

for the frequencies of interest. Let

$$\omega_{Q_4} = \nu\omega_{mx} \quad , \tag{5.6}$$

$$d_l = \hbar\omega_{mx}^2 D(Q_4, l\omega_{mx})/2\omega_{Q_4} = (l^2-\nu^2)^{-1} \quad , \tag{5.7}$$

and

$$\xi = \phi_{\backslash}^{(2)}\sum_{b_4}\left|U_x(Q_4)\right|^2 D(Q_4, l\omega_{mx})(\hbar/2m_{<}\omega_{Q_4})/d_l \quad . \tag{5.8}$$

Then, the ratio of the two vertices [Eq. (5.2)] becomes $3d_2\xi$, and the vertex renormalization factor is

$$\Lambda_3 = 1 + 3d_2\xi \quad . \tag{5.9}$$

Estimates of d_2 and ξ are provided in Sec. VI. It is easy to verify that (5.9) correctly accounts for all the three-phonon absorption processes shown in Fig. 4(c).

The reasoning used in this simple example can be applied to the general case to deduce the rules for writing down the renormalization factor for n-phonon absorption. The simplest term in the total vertex is the simple $(n+1)$-phonon vertex with one of the phonons being the fundamental mode driven at the optical frequency, as depicted by Fig. 5(a). A typical reducible vertex is formed by joining a number of irreducible vertices of lower order such that there is only one phonon line connecting any pair of irreducible vertices. Some examples are shown in Figs. 5(b)–5(d).

If a vertex contains m internal lines, then its ratio to the simple vertex [Fig. 5(a)] contains a factor ξ^m, with ξ defined by Eq. (5.8). Thus,

$$\Lambda_n = \sum_{m=0}^{n-2} S_{n\backslash}^{(m)}\xi^m \quad , \tag{5.10}$$

with the coefficient $S_n^{(m)}$ obtained as follows. Draw all topologically distinct reducible vertices with m

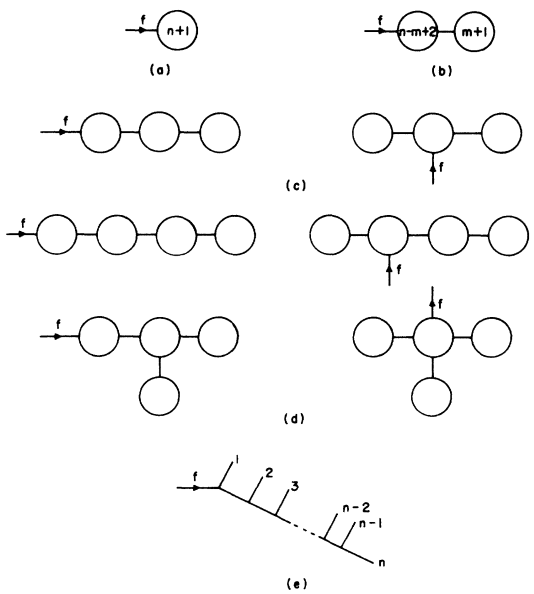

FIG. 5. n-phonon absorption vertices. The number n in a circle denotes a simple vertex with n external lines.

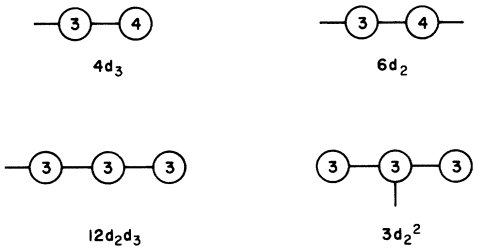

FIG. 6. Four-phonon absorption vertices. The only external line shown is the fundamental mode.

internal lines and $n+1$ external lines, one of which is the fundamental phonon driven at frequency $n\omega_{mx}$. Each diagram contributes to $S_n^{(m)}$ a term of the form

$$C_n^{(m)} d_{l_1} d_{l_2} \cdots d_{l_m} \quad , \tag{5.11}$$

where $C_n^{(m)}$ is the ratio of $n!$ to the number of ways of rearranging the states of the n outgoing phonon lines that do not change the reducible vertex. The factors of d_l come from the intermediate phonon lines, l being determined by energy conservation, assuming that all outgoing phonon lines have frequency ω_{mx}.

For example, the vertices with one internal line, as in Fig. 5(b), give

$$S_n^{(1)} = \sum_{m=2}^{n-1} \binom{n}{m} d_m \quad , \tag{5.12}$$

and Fig. 5(e) contributes to $S_n^{(n-2)}$ the term

$$(n!/2!) d_2 d_3 \cdots d_{n-1} \quad . \tag{5.13}$$

Armed with the general rules, we can calculate the contribution of any vertex. Figures 6–8 show the relevant vertices for four- to six-phonon absorption, respectively, and the corresponding contributions to $S_n^{(m)}$.

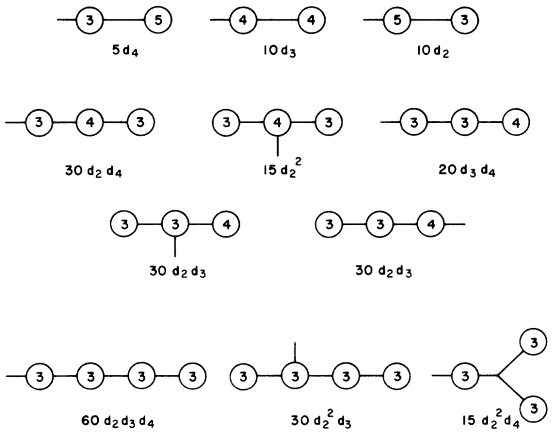

FIG. 7. Five-phonon absorption vertices.

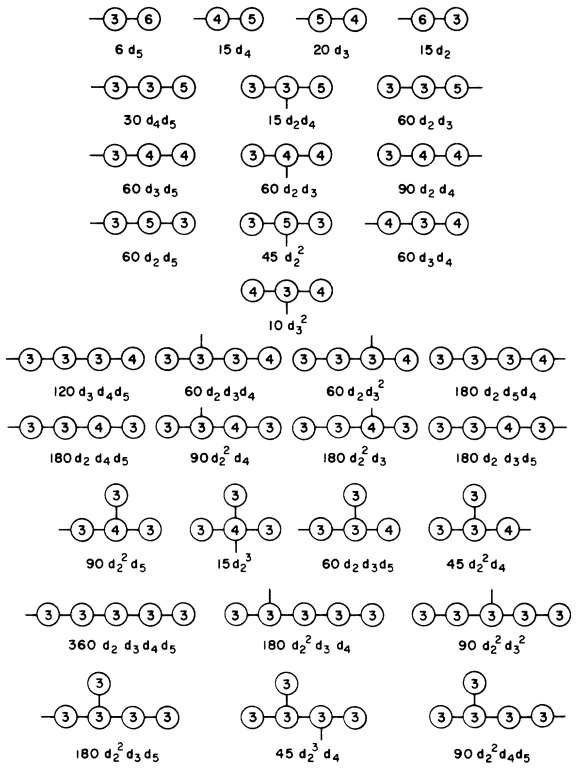

FIG. 8. Six-phonon absorption vertices.

From the considerations in Sec. VI the factor ν in Eq. (5.6) is 0.5 or less; thus (5.7) gives

$$d_l \simeq l^{-2} \quad . \tag{5.14}$$

Therefore, the vertex correction factors are

$$\Lambda_2 = 1, \quad \Lambda_3 = 1 + 0.75\xi,$$
$$\Lambda_4 = 1 + 1.9444\xi + 0.5208\xi^2 \quad ,$$
$$\Lambda_5 = 1 + 3.9236\xi + 2.6563\xi^2 + 0.3711\xi^3 \quad ,$$
$$\Lambda_6 = 1 + 7.1497\xi + 9.2682\xi^2 + 3.2511\xi^3 + 0.2806\xi^4 . \tag{5.15}$$

VI. FREQUENCY AND TEMPERATURE DEPENDENCE OF ABSORPTION COEFFICIENT

It is straightforward to evaluate β_n given by Eq. (3.7) with the α's given by the Brillouin-zone sums. We shall confine ourselves to two rough estimates of the α's.

For a linear-chain model with two atoms per unit cell, all with equal masses, it is possible to evaluate explicitly the α's in the low- and high-temperature limits. Table I shows the results for the α's with ω_{mx} chosen to be the top of the phonon spectrum. This simple model illustrates nicely all the important features that follow from Eq. (3.7). As a function of frequency, the absorption coefficient β_n due to the n-phonon–summation-process

TABLE I. Values of parameters from the diatomic-chain model with equal masses.

	α_{0+}	α_{1+}	α_{2+}	α_{0-}
Low T	$8/\pi$	$\frac{1}{4}\pi$	0.223	$8/3\pi$
High T	$4\omega_T/\omega_{mx}$	$2/\pi$	$[(\pi\omega_T/4\omega_{mx})-4/\pi^2]^{1/2}$	0

peaks near $n\alpha_{1+}\omega_{mx}$, which is about $\frac{3}{4}\, n\omega_{mx}$. Thus, the total absorption coefficient, which is the sum of all β_n with $n \geq 2$, is dominated at a particular frequency by the nearest-n-phonon summation process. The frequency dependence of β in the range $2\omega_{mx}-8\omega_{mx}$ is, therefore, approximately exponential since the strength of the peak in β_n as a function of n is approximately exponential. The small values of α_{0-} confirm the validity of neglecting Σ_{n-} in Eq. (3.7). As the temperature is raised, the strength of the peak in β_n increases, the position of the peak is shifted toward the lower frequency, and the width is either narrowed or broadened, depending on the temperature dependence of the phonon frequencies. Thus, β increases with temperature, but less rapidly than T^{n-1} at high temperatures.

Now we give a more realistic estimate for NaCl-structure crystals. There are several wave vectors for which the explicit expression of $|U_x(Q)|^2$ can be written down. For the acoustic branch at the zone boundary in the (1, 1, 1) direction, the light-mass ions stand still, and the heavy ions move in the direction $\hat{w}_{>Q}$, say. Then,

$$|U_x(Q)|^2 = (\hat{x}\cdot\hat{w}_{>Q})^2 m_</m_> \ . \tag{6.1}$$

Similarly, for the optical branch at the same wave vector,

$$|U_x(Q)|^2 = (\hat{x}\cdot\hat{w}_{<Q})^2 \ . \tag{6.2}$$

For the optical modes near the zone center, $U_x(Q)$ is given by Eq. (2.17). For the acoustical modes near the zone center, $|U_x(Q)|^2$ is nearly zero.

As a rough approximation, $|U_x(Q)|^2$ will be set equal to zero for $\omega < f\omega_{mx}$, where $f < 1$ and where it is not negligible, and $|U_x(Q)|^2$ will be approximated by an average of the three known expressions (2.17), (6.1), and (6.2); thus,

$$|U_x(Q)|^2 \simeq \tfrac{2}{9}(1+m_</m_>)\Theta(\omega_Q - f\omega_{mx}) \ , \tag{6.3}$$

where Θ is the unit step function. In the average, we have replaced $(\hat{x}\cdot\hat{w}_{<Q})^2$ by $\frac{1}{3}$, which is the value for the (1, 1, 1) zone-boundary mode and is also the angular average of $\cos^2\theta$. The remaining factor is the average of 1, $m_</m_>$, and $m_</m_r$.

The estimates of the α's are then, from (3.1), (3.2), (3.5), (3.6), and (6.3), with the usual approximation of the sum over Q by $6\int_0^\infty d\omega\, g(\omega)$,

$$\alpha_{0+} = \tfrac{4}{3}(1+m_</m_>)\langle(n+1)\Theta/\omega\rangle\omega_{mx} \ , \tag{6.4}$$

$$\alpha_{1+} = \langle(n+1)\Theta\rangle/\langle(n+1)\Theta/\omega\rangle\omega_{mx} \ , \tag{6.5}$$

$$\alpha_{2+}^2 = [\langle(n+1)\Theta\omega\rangle/\langle(n+1)\Theta/\omega\rangle\omega_{mx}^2] - \alpha_{1+}^2 \ , \tag{6.6}$$

where n is the Bose-Einstein distribution factor,

$$\langle A\Theta\rangle = \int_0^\infty d\omega\, g(\omega)A(\omega)\Theta(\omega - f\omega_{mx}) \ , \tag{6.7}$$

and $g(\omega)$ is the phonon density of states normalized to unity. Similar estimates give

$$\alpha_{0-} < \alpha_{0+}/(1+m_</m_>) \ . \tag{6.8}$$

The density of states, shown as the solid curve in Fig. 9, is approximated by the Debye model,

$$g(\omega) = (3\omega^2/\omega_{mx}^3)\Theta(\omega_{mx}-\omega) \ , \tag{6.9}$$

sketched as the dashed curve in Fig. 9. The value of ω_{mx} is taken as the Debye cutoff frequency in (6.9). In the high-temperature limit,

$$n(\omega)+1 \simeq \omega_T/\omega + \tfrac{1}{2} \ . \tag{6.10}$$

Then, the averages in Eqs. (6.4)–(6.6) are easily evaluated.

The value of f will be chosen as $f=\frac{1}{2}$, corresponding to the assumption that, for $\frac{1}{8}$ of the modes ($\frac{1}{4}$ of the acoustical modes), $W_+(Q)$ is negligible. In Table II, we list the data of NaCl along with the values of the α's at room temperature corresponding to $\omega_T/\omega_{mx} = 1.03$ for NaCl.

To estimate the magnitude of the vertex correction, we need to know the contribution of the intermediate phonon in the form of ξ given by Eq. (5.8). In the process depicted by Fig. 4(b), the intermediate phonon splits into two phonons Q_1 and Q_2, which were taken at frequency ω_{mx}, i.e., in the optical branches. This is reasonable since the

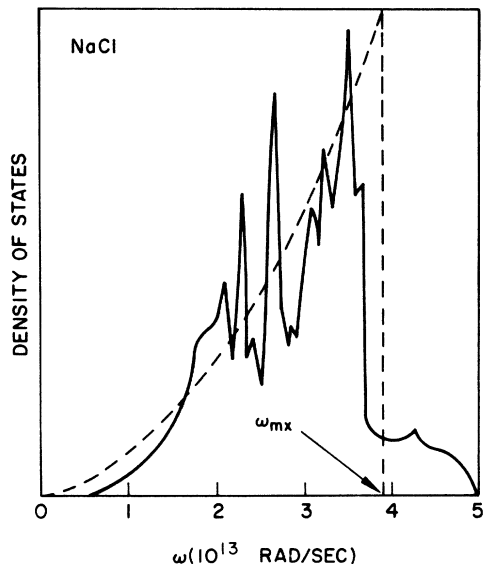

FIG. 9. Phonon density of states in NaCl and the Debye approximation.

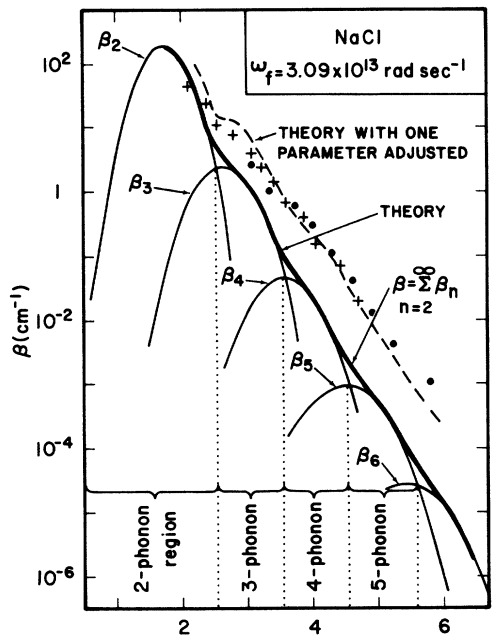

FIG. 10. Theoretical estimates of β_n at room temperature for NaCl. Experimental points from Fig. 1 are shown for comparison.

high-frequency side of the Gaussian $\beta_n(\omega)$ curves contribute to $\beta = \sum \beta_n$, as seen in Fig. 10. By a quasiselection rule,[10] Q_4 must be an acoustic mode, the largest contribution of which will be at the edge of the Brillouin zone. Thus, we take

$$|U_x(Q_4)|^2 \simeq \frac{1}{3}\frac{m_<}{m_>}\left(\frac{\omega Q_4}{\eta\omega_{mx}}\right)^2 \Theta(\eta\omega_{mx} - \omega_{Q_4}), \quad (6.11)$$

using Eq. (6.1). The frequency of the highest acoustic mode is taken to be $\eta\omega_{mx}$ with $\eta^3 = 0.5$, and the factor $(\omega_{Q_4}/\eta\omega_{mx})^2$ approximately simulates the effect of the polarization for the long-wavelength acoustic modes. Substituting Eq. (6.11) into Eq. (5.8), averaging over the possible modes of Q_4, and summing over three branches, we obtain an estimate of ξ:

$$\xi \simeq 3\phi^{(2)}/5m_>\omega_{mx}^2 \simeq 0.18 \ . \quad (6.12)$$

Substituting this value into Eq. (5.15) yields the following estimates for the vertex-renormalization factors:

$$\Lambda_2^2 = 1; \quad \Lambda_3^2 = (1+0.142)^2 = 1.30;$$

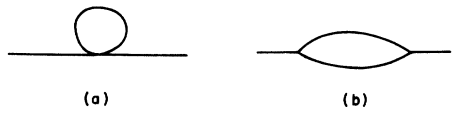

FIG. 11. Phonon self-energy terms of order ϵ^2.

TABLE II. Values of parameters for NaCl at room temperature.

α_{0+}	α_{1+}	α_{2+}
4.639	0.757	0.145

$\rho = 1/9.05$, $a = 2.82$ Å, $B = 2.44 \times 10^{11}$ dyn/cm^2,
$\omega f = 3.09 \times 10^{13}$ sec^{-1}, $\omega_{mx} = 3.85 \times 10^{13}$ sec^{-1},
$n_r = 1.50$ (formally for all ω), $m_< = 3.82 \times 10^{-23}$ g,
$m_> = 5.89 \times 10^{-23}$ g.

$$\Lambda_4^2 = (1+0.388)^2 = 1.93; \quad \Lambda_5^2 = (1+0.844)^2 = 3.40;$$
$$\Lambda_6^2 = (1+1.72)^2 = 7.38 \ . \quad (6.13)$$

We note that, from Eqs. (5.1) and (5.2), the vertex ratio can be shown to be equal to the ratio of the real parts of the self-energy terms given by Figs. 11(a) and 11(b) at zero temperature and frequency $2\omega_{mx}$. From R. A. Cowley's calculation[13] for KBr, our estimate of ξ appears to be somewhat too large.

The multiphonon absorption calculated from (3.7) using the values of parameters from Eq. (6.13) and Table II is shown in Fig. 10, where the individual β_n are plotted as light curves and the sum of the β_n is plotted as the heavy curve. The agreement is rather good in view of the crude approximations used to estimate the α's. It should be noted that no parameters have been adjusted in the theoretical result.

By adjusting two parameters in Eq. (3.7), such as K and D_e (keeping the α's at $f = \frac{1}{2}$), the experimental data can be fitted to within the scatter of the data. In fact, by changing only the value of the single-interaction strength parameter $1/\rho$ from 9.0 to 12, the dashed curve in Fig. 10 is obtained. This larger value could be partly explained by the fact that the higher-order anharmonic coefficients are much more sensitive to the shape of the potential curve than the quadratic terms from which the value of ρ is determined. Errors introduced by the approximations and uncertainties in the values of the parameters used also could account for the difference, of course.

The near-exponential frequency dependence is evident in Fig. 10. The vertex correction, which is included in Fig. 10, slightly improves the agreement with the experimental result. Without this correction, the β_2-β_5 curves would be shifted down by factors of 1, 1.3, 1.9, and 3.4, respectively.

The n-phonon regions, marked on Fig. 10, do not correspond to $n\omega_f < \omega < (n+1)\omega_f$, to $n\omega_{mx} < \omega < (n+1)\omega_{mx}$, or to $n\omega_{LO} < \omega < (n+1)\omega_{LO}$, as is often assumed in the literature. In fact, the n-phonon regions shift as the temperature changes, as discussed below.

The $n = 2$ central-limit curve is included in Fig.

10 even though its accuracy is not expected to be good. The two-phonon structure is lost, of course, in approximating β_2 by a Gaussian, and the peak does not occur at $\omega = \omega_f$.

The temperature dependence of β at a given frequency in the nearly exponential region is considerably weaker[25] than that of the simple expression

$$\beta_n(T)/\beta_n(0) = (1 - e^{-\omega/\omega_T})(1 - e^{-\omega/n\omega_T})^{-n} \sim T^{n-1} \tag{6.14}$$

obtained formally from the occupation-number factor (2.4) by setting all $\omega_Q = \omega/n$. The approximation $\beta_n \sim T^{n-1}$ in (6.14) is valid in the high-temperature limit, and n has been assumed to be independent of temperature in the past. The T dependence of β results from the temperature dependence of the parameters a, e^*, and, particularly, the phonon frequencies ω_Q and from the explicit temperature dependence of α_{0+}, α_{1+}, and α_{2+}.

The following example of NaCl at 300 K and 10.6 μm illustrates the strong deviation from the frequently quoted result $\beta \sim T^{n-1}$. The value of the slope $(T/\beta)d\beta/dT$ of β as a function T on a log-log plot can be estimated from Eq. (3.7). Using $n = 5.5$ from Fig. 10 and the following approximate expressions for the temperature dependence of the parameters,[26,27] $\omega_Q = \omega_{Q0}(1 - 3.8\times10^{-4}T)$, $a = a_0(1 - 4.4 \times 10^{-5}T)$, and $e^* = e_0^*(1 - 1.06\times10^{-4}T)$, we find

$$\frac{T}{\beta}\frac{d\beta}{dT} = 2.5\,, \tag{6.15}$$

which is considerably smaller than $n - 1 = 4.5$. The Born-Mayer-potential parameters C and $\rho_K \equiv \rho a$ in (2.11) are essentially temperature independent, being electronic in nature. In particular, Eq. (2.12) should not be used to ascribe a temperature dependence to ρ_K from measured values of $B(T)$ and $a(T)$. The temperature dependence of B arises from anharmonic and volume effects, not from a T dependence of ρ_K.

A weakening of the temperature dependence such as that in (6.15) is apparent in the data of Harrington and Hass,[25] Barker,[8] Kaiser and co-workers,[8] and Denham and co-workers.[8] Finally, it is mentioned that in a material, possibly a zinc-blende-structure crystal, in which the position of a given multiphonon peak can be traced as a function of temperature, the temperature dependence should be quite different from that of β at a given frequency. A detailed presentation of the temperature dependence of β will be given elsewhere.

The $\beta - \omega$ curves of the alkali halides and alkaline earths show less structure than those of the semiconductor materials. It is plausible that the greater anharmonicity of the NaCl-structure crystals could give rise to such short lifetimes of the zone-boundary phonons that the fine structure in the density of states is essentially eliminated.

The lifetime of the fundamental phonon is short,[13,28] and the lifetimes of the zone-boundary phonons should be even shorter since the selection rules and quasi-selection rules do not apply to the zone-boundary modes (with nonzero wave vectors). A value of relative linewidth $2\Gamma/\omega$ of the order of 0.3 for the zone-boundary phonons at resonance should be sufficient, and this value is reasonable in view of the value[28] of $2\Gamma/\omega = 0.07$ for the fundamental mode in NaCl and the fact that $2\Gamma/\omega$ is expected to be larger at the zone boundaries. Furthermore, as n becomes larger, more convolutions are involved [see Eq. (3.3)], and each convolution tends to smooth out any fine structure in the density of states.

This explanation is consistent with the experimental results which show that the two-phonon peaks are wider in the alkali halides than in the semiconductor materials, that $\Gamma \sim T^2$ at the fundamental resonance in NaCl (implying that the two-phonon contribution is small at resonance), and that the two-phonon peaks have been observed in NaCl even though $\Gamma \sim T^2$ at resonance. A careful study of the temperature dependence of the two-phonon summation peaks could show an increase in the widths of the peaks as T is raised from 77 K to the highest practical temperature of the solid. Such increases are apparent in the small amount of existing data.[29] As the temperature is reduced below room temperature, additional multiphonon peaks could appear in higher-n regions where $\beta(\omega)$ is relatively smooth at room temperature. Of the three existing known cases (for CaF_2, BaF_2, and SrF_2 at 77 and 300 K),[29] two show a small additional peak at 77 K that is absent at 300 K.

It should be emphasized that the two-phonon peaks are associated with peaks in the appropriate density of states and are not resonance lines. Thus, an extrapolation of $\beta(\omega)$ from the reststrahl region should *not* be subtracted from β at higher frequencies to obtain the multiphonon contribution, as is sometimes done in the literature. An alternate, though unlikely, explanation of the lack of structure is that the raw-phonon density of states shows little structure.

VII. ASSUMPTIONS AND APPROXIMATIONS

The assumptions and approximations made in the previous sections are now summarized: (i) The photon-phonon coupling is given by the leading dipole term, and the Lax-Burstein-Born mechanism[9] is neglected. (ii) For the anharmonic forces, only the nearest-neighbor Born-Mayer repulsion term is included and is further approximated. (iii) The lifetimes of the intermediate- and final-state phonons are assumed to be infinite. (iv) The central-limit theorem is used to reduce the n-fold multiple sum in (2.3) to a Gaussian whose parameters α are

given by single sums, although it is possible to improve the asymptotic approximation.[20] (v) Rough estimates were given for the various Brillouin-zone sums over the phonon coordinates for the coefficients α's. All of these approximations except (i) were shown to be reasonable. The perturbation approach used is justified by showing that all diagrams not included in the results are negligible. Concerning (i), the long-standing question of the importance of the Lax-Burstein-Born mechanism in NaCl-structure materials remains unanswered. The mechanism is quite simple to include formally; estimating the strengths of vertices has been the problem.

Our calculation gives good agreement with experimental results for the frequency dependence of the optical absorption and demonstrates the general nature of this dependence for crystals with tetrahedral symmetry. The estimates listed in (v) above enable us to see explicitly the nature of our results. Some of the estimates must be regarded as tentative. However, these approximations are not essential to our theory. We plan to perform both the multiple sums in (2.21) for $n=2-6$ and the single-phonon sums in Eqs. (3.2), (3.5), (3.6), and (5.8) by computer. This will enable us to examine more rigorously the validity of the other approximations, especially (iv). The computer results for the multiple sums in (2.21) should provide greater accuracy in the small-n regions, say $n=2$ and 3, where the central-limit results are less accurate, and should afford a good test of the approximations in the region of $n=4-6$. The temperature and frequency dependence of β for a number of crystals will be included in the computer program, which is being performed in collaboration with A. Karo of the Lawrence Livermore Laboratory.

---

*Research supported by the Advanced Research Projects Agency of the Department of Defense and was monitored by the Defense Supply Service-Washington, D.C. under Contract No. DAHC15-73-C-0127.

[1]E. Burstein, *Lattice Dynamics*, edited by R. F. Wallis (Pergamon, Oxford, England, 1965), p. 315.

[2]D. H. Martin, Adv. Phys. **14**, 39 (1965).

[3](a) H. Bilz, *Phonons in Perfect Lattices*, edited by R. W. H. Stevenson (Oliver and Boyd, Edinburgh, Scotland, 1966), p. 208; (b) R. A. Cowley, in Ref. 3(a), p. 192.

[4]W. G. Spitzer, *Semiconductors and Semimetals*, edited by R. K. Wilkinson and A. C. Beer (Academic, New York, 1967), Vol. 3, p. 17.

[5]L. Van Hove, Phys. Rev. **89**, 1189 (1953); J. C. Phillips, Phys. Rev. **104**, 1263 (1956).

[6]G. Rupprecht, Phys. Rev. Lett. **12**, 580 (1964).

[7](a) F. A. Horrigan and T. F. Deutsch, Raytheon Res. Div., Quarterly Techn. Rept. Nos. 1 and 2, 1972 (unpublished). (b) *American Institute of Physics Handbook*, 3rd ed., edited by D. E. Gray (McGraw-Hill, New York, 1972); (c) C. Smart, G. R. Wilkinson, A. M. Karo, and J. R. Hardy, *Lattice Dynamics*, edited by R. F. Wallis (Pergamon, New York, 1965), p. 387; (d) L. Genzel, Festkoerperprobleme **VI**, 32 (1966).

[8]W. Kaiser, W. G. Spitzer, R. H. Kaiser, and L. E. Howarth, Phys. Rev. **127**, 1950 (1962); P. Denham, G. R. Field, P. L. R. Morse and G. R. Wilkinson, Proc. R. Soc. A **317**, 55 (1970); A. J. Barker, J. Phys. C **5**, 2276 (1972).

[9]M. Lax and E. Burstein, Phys. Rev. **97**, 39 (1955).

[10]M. Sparks and L. J. Sham, Solid State Commun. **11**, 1451 (1972); M. Sparks and L. J. Sham, Conference on High Power Infrared Laser Window Materials, Hyannis, Mass., 1972 (Air Force Cambridge Research Laboratories, Cambridge, Mass., to be published); M. Sparks, Fourth ASTM Damage in Laser Materials Symposium, Boulder, Colo., 1972 (unpublished); M. Sparks, Xonics, Inc. Technical Progress Reports, 1972 and Final Report, 1972, under Contract No. DAHC15-72-C-0129 (unpublished).

[11]R. F. Wallis and A. A. Maradudin, Phys. Rev. **125**, 1277 (1962).

[12]M. Born and K. Huang, *Dynamical Theory of Crystal Lattices* (Oxford U. P., Oxford, England, 1954).

[13]R. A. Cowley, Adv. Phys. **12**, 421 (1963); E. R. Cowley and R. A. Cowley, Proc. R. Soc. A **287**, 259 (1965); E. R. Cowley, J. Phys. C **5**, 1345 (1970).

[14]P. N. Keating and G. Rupprecht, Phys. Rev. **138**, A866 (1965).

[15]B. Szigeti, *Lattice Dynamics*, edited by R. F. Wallis (Pergamon, Oxford, England, 1965), p. 405.

[16]M. Sparks, *Ferromagnetic Relaxation Theory* (McGraw-Hill, New York, 1964).

[17]C. Kittel, *Introduction to Solid State Physics, 4th ed.* (Wiley, New York, 1971).

[18]A. A. Maradudin, E. W. Montroll, G. H. Weiss, and I. P. Ipatova, *Theory of Lattice Dynamics in the Harmonic Approximation*, 2nd ed. (Academic, New York, 1971).

[19](a) A. A. Maradudin and S. H. Vosko, Rev. Mod. Phys. **40**, 1 (1958); (b) T. McGill, R. Hellwarth, M. Mangir, and H. Winston (private communication); (c) D. L. Mills and A. A. Maradudin (private communication); (d) B. Bendow, S. C. Ying, and and S. P. Yukon (private communication).

[20]H. Cramer, *Methods of Statistics* (Princeton U. P., Princeton, N. J., 1946), Chap. 17; and *Random Variables and Probability Distribution*, 2nd ed. (Cambridge, U. P., Cambridge, England, 1961), p. 87.

[21]A. Sjolander, Ark. Fys. **14**, 315 (1958).

[22]L. Van Hove, *Problems in Quantum Theory of Many-Particle Systems* (Benjamin, New York, 1961).

[23]A. A. Maradudin and A. E. Fein, Phys. Rev. **128**, 2589 (1962).

[24]G. Raunio and S. Rolandson, Phys. Rev. B **2**, 2098 (1970).

[25]J. Harrington and M. Hass (private communication).

[26]R. T. Harley and C. T. Walker, Phys. Rev. B 2, 2030 (1970).

[27]A. M. Karo (private communication).

[28]R. B. Barnes and M. Czerney, Z. Phys. 72, 477 (1931).

[29]See Figs. 5 (for CaF_2) and 8 (for SrF_2) of Ref. 8, Denham *et al.* for results at 100 and 300 K.